Alteration of nociceptive Schwann cells in a mouse model of peripheral neuropathy in prediabetic condition

Guillaume Rastoldo[1], Ali K. Jaafar[1], Aurélie-Paulo-Ramos[1], Katy Thouvenot[1], Cynthia Planesse[1], Matthieu Bringart[1], Marie-Paule Gonthier, Gilles Lambert and Steeve Bourane[1]*

1- Université de La Réunion, INSERM, UMR 1188 Diabète athérothrombose Réunion Océan Indien (DéTROI), Saint-Pierre, La Réunion, France.

Abstract

Diabetic peripheral neuropathy (DPN) characterized by progressive and symmetrical sensory abnormalities is one of the earliest and main complications of diabetes. DPN is characterized by heterogeneous sensory symptoms such as chronic pain, tingling, burning or loss of sensation. Nociceptive Schwann cells (nSCs), a recently identified subtypes of dermal Schwann cells support terminal nerve fibers in mouse skin and contribute to mechanical sensation and neuropathic pain. While terminal nerve fibers density is basically evaluated in DPN models, there is currently few data about nSCs number and integrity during early stage of DPN. In the present study, we used a mouse model of prediabetes by using high-fat diet (HFD) fed mice to determine if there are quantitative differences in terminal nerve fiber density, nSCs number and cellular extensions between control and prediabetic neuropathic mice. In this study, we identified L1CAM as a reliable marker of nSCs currently characterized by the expression of S100β and Sox10. Interestingly, we observed a decrease in intraepidermal nerve fiber density (IENFD) associated to a significant reduction of nSCs in the glabrous foot skin of neuropathic mice. Overall, this study identifies L1CAM as a new marker of nSCs and indicates that these cells are impaired during prediabetic peripheral neuropathy.

Keywords: DPN; Nociceptive Schwann Cells; Type 2 diabetes; Mechanical hypoalgesia; Thermal hyperalgesia

Introduction

Diabetes is one of the most prevalent chronic diseases in the world. The epidemic threshold has been reached with over 537 million people affected worldwide. According to estimates by the International Diabetes Federation, this number is expected to reach 783 million patients by 2045. One of the first and main complications of diabetes is diabetic peripheral neuropathy (DPN), affecting more than 60% of diabetic patients (Feldman et al., 2017). Prediabetes represents the early stages of glucose dysregulation and precedes the development of type 2 diabetes. Prediabetes and diabetes are the most common causes of peripheral neuropathy in Europe and the United States (Feldman et al., 2017). DPN involves damage to the peripheral nervous system, i.e., the sensory and motor nerves as well as the autonomic nervous system that controls our organs. The most common symptoms of DPN are an impairment of sensitivity to pain and touch (Themistocleous et al., 2016). The early stages of the pathology is characterized by abnormal sensory symptoms such as pain, tingling, burning sensations, electrical discharges, pain evoked by non-painful mechanical stimuli (allodynia), increased sensitivity to noxious stimuli (hyperalgesia) (Themistocleous et al., 2016) significantly altering the patients' quality of life. These symptoms are difficult to treat with conventional analgesics.

Other sensory deficits such as numbness are also observed with progressive loss of sensation in the lower limbs often leading to tissue damage with the development of ulcers, increasing the risk of amputation (Callaghan et al., 2012a). Diabetes is the leading cause of lower extremity amputations, with a 15-fold increase in risk compared with non-diabetic populations (Margolis et al., 2011). Reduced sensation in the feet also leads to progressive loss of balance resulting in an increased risk of falls, fractures and death (Green et al., 2010; Malik et al., 2005).

Despite decades of research, there is currently no effective treatment for DPN due to an incomplete understanding of its mechanisms and key players. Much attention in DPN studies has been dedicated to the damage of small, non-myelinated nerve fibers (C-fibers) responsible for sensitivity to heat and pain. The degeneration and regeneration of these C-fibers are typically associated with diabetic patient phenotypes. Skin biopsy analysis in clinic serves as a late-stage confirmation of DPN presence (Lauria et al., 2022), lacking a diagnostic tool for predicting C-fiber degeneration related to pain.

While C-fibers was traditionally believed to terminate freely in the epidermis, recent work by Abdo et al. challenges this perception (Abdo et al., 2019). Their findings reveal a close connection between these C-fibers and specialized nociceptive Schwann cells (nSC) capable of independently generating pain signals. These cells are currently identified by the expression of S100β and Sox10 (Hu et al., 2022; Ojeda-Alonso et al., 2023; Rinwa et al., 2021). Conversely, eliminating these nSC alone seems sufficient to induce neuropathic pain in mice (Rinwa et al., 2021). Considering these recent discoveries, it is conceivable that neuropathies involving C-fiber degeneration, as seen in DPN, may result from early damage to nSCs. A recent report

supports this hypothesis and demonstrated a decreased in nSC density in Streptozotocin-induced type 1 diabetes mice (Hu et al., 2022). However, no study has evaluated the integrity of nSC in a type 2 diabetes model such as HFD or in prediabetes conditions.

To explore this hypothesis, our research delves into the impact of prediabetes on the integrity of nSC during pathology development, an aspect that remains unexplored in the realm of DPN investigations.

Methods

Research Design

All reported experiments were performed at the GIP-CYROI platform's animal facility, conducted in accordance with the French and European Community Guidelines for the Use of Animals in Research (86/609/EEC and 2010/63/EU), and were approved by the local Ethics Committee (n°114) for animal experimentation and the French authorities (APAFIS#31763-2018020912188806, approved on May 21, 2021).

Animals

Twenty C57BL/6J mice (male, 6 weeks old) were purchased from Janvier (Le Genest Saint Isle, France) and housed with 5 mice per cage in a temperature-controlled environment with a 12–12h light/dark photocycle. After 2 weeks of adaptation, mice were divided in two groups (n=10/group) and placed on either a control diet (10% kcal %fat; SF13-081) or a high-fat diet (45% kcal %fat; SF04-001) from Specialty Feeds during 16 weeks.

Transgenic mouse line and Tamoxifen injection

Mice expressing a tamoxifen-inducible Cre recombinase under the control of the PLP promoter (PLP-CreER^{T2}; (Leone et al., 2003)) were crossed to Ai14 mice, which have a LoxP-flanked stop cassette excisable by Cre. At 6 weeks old, the PLP-CreER^{T2}; Ai14 progeny were injected intraperitoneally with tamoxifen (100 µg/g of mice) for 5 consecutive days. Tamoxifen was prepared in a mixture of 9/10 corn oil and 1/10 ethanol, and stored at 4 °C in a light-proof container. After 2 weeks, the mice were euthanized and the tissue collected for immunostaining.

Genotyping

101 Genotyping of progeny from PLP-CreER^{T2} and Ai14 mice were done with PCR using CreDN2
102 (GAT CTC CGG TAT TGA AAC TCC AGC), CreUP2 (GCT AAA CAT GCT TCA TCG TCG G), Ai14mut-
103 Fwd (CTG TTC CTG TAC GGC ATG G) and Ai14mut-Rev (GGC ATT AAA GCA GCG TAT CC).

104

105 **Oral glucose tolerance test (OGTT)**

106 An OGTT was performed after 16 weeks of diet in all mice. After 6 hours of fasting, one drop
107 of tail blood was collected and glycemia was analyzed using a standard glucometer (One Touch
108 Profile, Lifescan Inc., Milpitas, CA, USA, #6 strips). Oral gavage with glucose 30% (2g/kg body
109 weight) into conscious mice was performed and glycemic levels measured after 15, 30, 45, 60,
110 90 and 120 min post-administration.

111

112 **Nerve conduction velocity**

113 Mice were anesthetized by using isoflurane (IsoFlo®, Centravet, France) and placed on a
114 heating pad. Once they were deeply anesthetized, motor nerve conduction velocities (MNCV)
115 and sensory nerve conduction velocities (SNCV) were determined as previously described
116 (Obrosova et al., 2004; Oh et al., 2010; Schulz et al., 2014). Using the Keypoint 4, Dantec-
117 Medtronic electroneuromyography device, we performed both proximal and distal nerve
118 stimulations of the sciatic nerve, registering the transmitted potentials with sensing
119 electrodes at the gastrocnemius muscle. We used stainless steel subdermal needle electrodes
120 to deliver single square-wave supramaximal stimulation with 0.2 millisecond impulses. MNCV
121 was calculated by subtracting the distal from the proximal latency (measured in milliseconds)
122 from the stimulus artifact of the take-off of the evoked potential, and the difference was
123 divided into the distance between both stimulating electrodes (measured in millimeters using
124 a Vernier caliper). For SNCV, recording electrodes were placed on the dorsum of the foot and
125 stimulating electrodes on the ankle. For SNCV, the latency of onset (milliseconds) of the
126 sensory nerve action potential after supramaximal antidromic stimulation of the sural nerve
127 at the ankle was divided by the distance between the recording and stimulation electrodes
128 (measured in millimeters using a Vernier caliper).

129

130 **Tissue Harvest**

131 After 16 weeks of diet, mice received a subcutaneous injection of Buprenorphine (0.05 mg/kg,
132 Buprecare®, Centravet, France) and were anesthetized by using isoflurane (3%). The mice were
133 then euthanized by intracardiac puncture and blood samples were collected into Eppendorf
134 tubes and centrifuged at 2000 rpm for 10 min at 4°C. Serum was collected and stored at −80°C
135 until analysis. Intracardiac perfusion was performed with 20 mL of phosphate buffered saline
136 (PBS) and 20 mL of 4% paraformaldehyde (PFA) dissolved in PBS. The hind-paw plantar
137 surfaces of each mouse were collected and post-fixed overnight in 4% PFA solution. Biopsies

138 of foot skin were then rinsed and cryoprotected into 30% sucrose dissolved in PBS at 4°C. The
139 samples were then embedded in optimal cutting temperature (OCT, Tissue-Tek®, USA)
140 compound and stored at −80°C until sectioning.

141

142 **Immunohistochemistry**

143 Tissus sections (30 µm) were collected from the hind-paw plantar surface and washed
144 (3x10min) with PBS. Blocking and permeabilization were done by incubation (1h) in 5% donkey
145 anti-serum and 0.3% Triton X-100. For intraepidermal nerve fibers density, sections were
146 incubated with the primary antibody anti-PGP9.5 (1:500, #14730-1-AP, ProteinTech) for 2
147 days; first overnight at 4°C and the next day sections were incubated overnight at room
148 temperature. The same protocol was applied for L1 cell adhesion molecule (L1CAM, 1:500,
149 #20659-1-AP, ProteinTech) antibody but the sections were incubated only overnight at 4°C.
150 Sections were then rinsed in PBT (PBS + 0.1% triton) and incubated for 1 h at room
151 temperature with the secondary antibody Alexa Fluor 594 donkey anti-rabbit (1:500, Abcam;
152 ab150064), or Alexa Fluor 488 donkey anti-Rabbit (1:500, Invitrogen; A-21206).

153

154 **Identification and quantification of nociceptive Schwann cells**

155 Nociceptive Schwann cells were identified according to Hu et al. criteria (Hu et al., 2022).
156 Briefly, positive staining of S100β, Sox10 and DAPI identified nSCs. However, our investigation
157 revealed that the traditional markers for nociceptive Schwann cells (S100β and Sox10)
158 exhibited colocalization with L1CAM staining (**Supplementary Figure 1A**). Furthermore,
159 L1CAM staining colocalized with Td-tomato expression in a tamoxifen-induced PLP-*Cre*ER^{T2};
160 R26TdTomato double transgenic mouse (**Supplementary Figure 1B**). Cre-mediated
161 recombination driven by the proteolipid protein 1 (Plp1) promoter is employed specifically to
162 target Schwann cells (Doerflinger et al., 2003; Gomez-Sanchez et al., 2017; Grove et al., 2017).
163 These findings confirm that L1CAM is a reliable marker of nociceptive Schwann cells and can
164 independently be used without S100β and Sox10 to identify these cells.

165 To quantify nSCs, their localization within the foot skin is important. Commonly, nSCs connect
166 to PGP9.5+ nerve endings and are located within 25 µm depth in the subepidermal zone at
167 the junction between dermis and epidermis. For quantification, we exclude L1CAM positive
168 staining in glands or large peripheral fiber bundles found deeper in the dermis. The number
169 of nSCs was reported per mm length of foot skin.

170 To quantify nSCs cellular extensions, we measured cell fluorescence using ImageJ. We selected
171 the region of interest (ROI) at the subepidermal zone in each image of the foot skin and
172 measured the mean fluorescence value in that area using 'Mean gray value'.

173

174 **Confocal imaging**

175 Intraepidermal nerve fibers density and nociceptive Schwann cells number were evaluated
176 under a laser scanning confocal microscope Eclipse (Nikon) with a 40x objective. Following
177 immunostaining, 30 µm thick Z-stack images were taken and analysis was performed on
178 orthogonal maximum intensity projection of the original confocal Z-stack images.

179

180 **Metabolic markers**

181 Plasma hemoglobin A_1C levels were determined using DCA® Vantage Analyzer (Siemens
182 Healthineers, France) and hemoglobin A_1C reagent kit (#23-312018). Serum triglycerides (TG)
183 and total cholesterol levels were determined using colorimetric assays (Diasys®,
184 #157109910021 and #113009910021, Germany). Plasma insulin and leptin concentrations
185 were measured using a mouse insulin and leptin ELISA kit (Mercodia®, #10-1247-01, Sweden
186 and RayBiotech®, Peachtree Corners, GA, USA). All metabolic markers were measured after
187 16 weeks of diet.

188

189 **Behavioral tests**

190 *Von Frey test*

191 Mice were habituated to the testing apparatus for 1h/day during a week before behavioral
192 testing. After this acclimation, animals were placed on an elevated wire grid and the plantar
193 surface of the hindpaw was stimulated with calibrated von Frey monofilaments (0.008-6 g).
194 The paw withdrawal threshold for the von Frey assay was determined by SUDO up-down
195 method (Bonin et al., 2014). Testing was performed every 4 weeks after the start of the diet
196 and up to 16 weeks.

197

198 *Hargreaves test*

199 To measure radiant heat pain by Hargreaves test (Hargreaves et al., 1988), animals were put
200 in plastic boxes and the plantar paw surface was exposed to a beam of radiant heat according
201 to the Hargreaves method. Paw withdrawal latency was then recorded and beam intensity
202 was adjusted to result in a latency around 10 seconds in control animals. High speed of skin
203 heating (6.5°C/sec) preferentially activates Aδ-fibers (Yeomans and Proudfit, 1996). Based on
204 the study of Deuis and Vetter (Deuis and Vetter, 2016), we can assume that we used a medium
205 to high speed of temperature heating (5°C/sec during 10 sec to obtain 50°C) which could
206 indicate a predominant activation of Aδ-fibers on this behavioral test. Testing began after
207 exploration and grooming behaviors ended. The heat stimulation was repeated 5 times at an
208 interval of 10 min for each animal and the mean was calculated. A cutoff time of 30 seconds
209 was set to prevent tissue damage. Testing was performed every 4 weeks after the start of the
210 diet and up to 16 weeks.

211 *Brush Test*

212 To measure dynamic allodynia, mice were habituated to the testing apparatus (the same that
213 for von-Frey test) for 1h/day during a week before behavioral testing. After this acclimation,
214 a soft paintbrush (Lefranc & Bourgeois® - Brush no. 4 #175160) was used to gently stroke the
215 plantar surface of the hindpaw in the direction from heel to toe. The test was repeated five
216 times, with intervals of 5 min. For each test, no evoked movement was scored as 0, and
217 walking away or occasionally brief paw lifting (~1 sec or less) was scored as 1. For each mouse,
218 the cumulative scores of the five tests were used to form a percentage response (100%
219 response equivalent to 5 evoked movements during the 5 stimulations of the paw). Testing
220 was performed every 4 weeks after the start of the diet and up to 16 weeks.

221 *Pinprick Test*

222 To measure acute mechanical pain, mice were habituated to the testing apparatus (the same
223 that for von-Frey test) for 1h/day during a week before behavioral testing. After this
224 acclimation, for pinprick test, we touched the plantar surface of the hindpaw with a pin
225 (Bourane et al., 2015) and measured numbers of withdrawal response as for the brushing
226 tests. For each mouse, the cumulative scores of the five tests were used to form a percentage
227 response (100% response equivalent to 5 evoked movements during the 5 stimulations of the
228 paw). Testing was performed every 4 weeks after the start of the diet and up to 16 weeks.

229

230 **Statistical analysis**

231 We first analyzed the normality of all the data and showed that the results of serum
232 triglycerides and total cholesterol levels, insulinemia, motor NCV, sensory NCV, IENFD and
233 L1CAM-positive cells were normally distributed. Thus, unpaired Student's *t*-tests (two tailed)
234 were used for statistical comparisons. For behavioral data, a two-way ANOVA for repeated
235 measures followed by Bonferroni's post-hoc test was used to determine statistically significant
236 differences. A *P* value of less 0.05 was considered significant.

237

238

239 ## Results

240 1. *Body weight gain, serum triglycerides and total cholesterol levels*

241 In order to determine the effect of high-fat diet (HFD) on the development of peripheral
242 neuropathy, we fed mice with a control diet (10% kcal %fat) or a HFD (45% kcal %fat) for 16
243 weeks (n=10/group, **Figure 1A**). As expected, HFD-fed mice gained significant weight
244 compared to control diet-fed mice. The difference became significant from week 11 onward
245 (**Figure 1B**). Mice on the control diet gradually gained 10 g in body weight, whereas HFD-fed
246 mice gained 18 g over the course of the study. In line with weight gain, blood samples analysis

247 revealed that HFD-fed mice exhibited higher circulating levels of leptin compared to control
248 diet-fed mice (**Figure 1C**).Triglycerides levels were not significantly altered (**Figure 1D**).
249 However, HFD-fed mice showed significantly higher total plasma cholesterol level than mice
250 fed with the control diet (P < 0.01; **Figure 1E**).

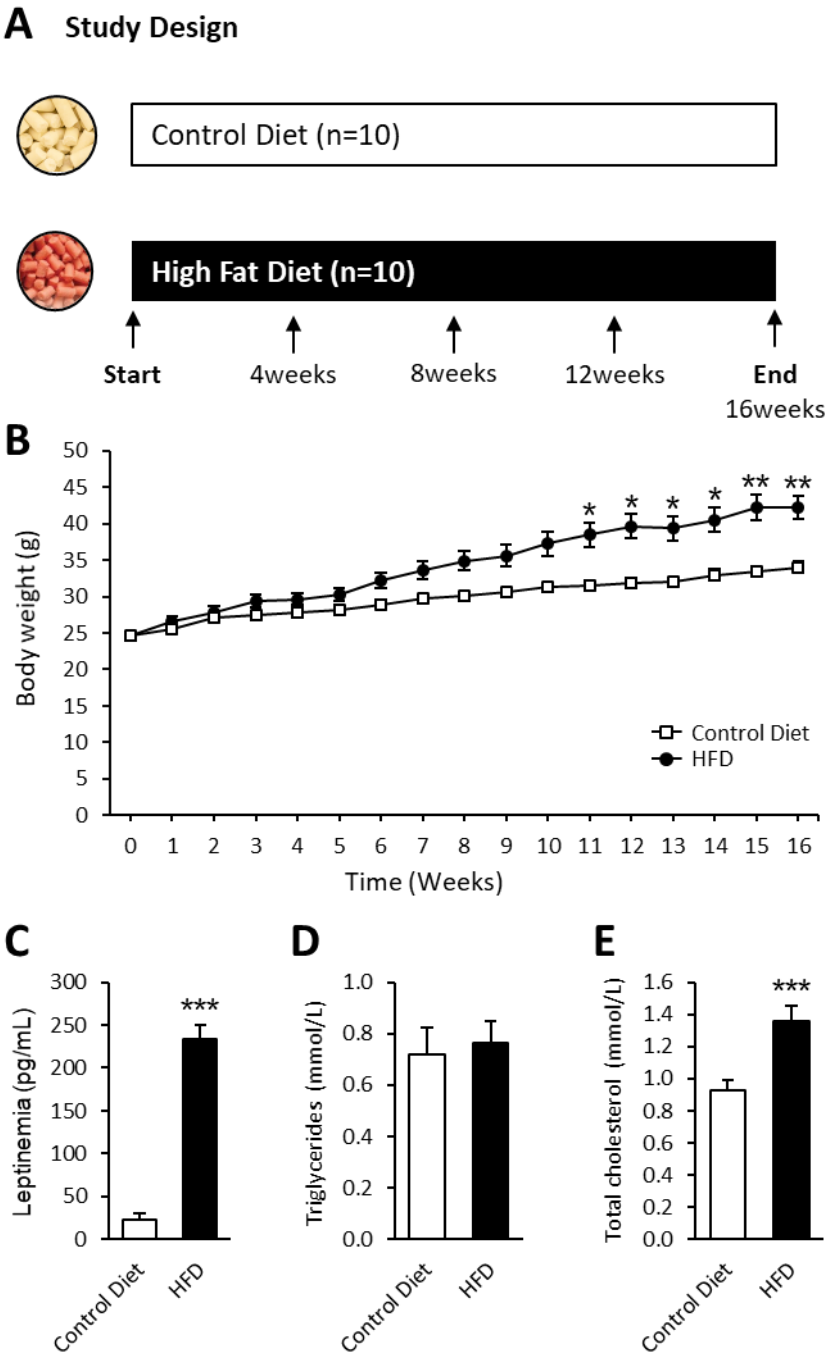

251

252 **Figure 1: Study design and HFD-induced dyslipidemia.** (**A**) Study Design used to assess the effect of a
253 HFD (45% kcal %fat) vs. a control diet (10% kcal %fat) in two groups of mice (n=10/group). (**B**) Body
254 weight of control diet-fed mice and HFD-fed mice during the 16 weeks of diet. (**C**) Leptinemia of control
255 and HFD mice at 16 weeks of diet. (**D**) Plasma levels triglycerides of control and HFD mice at 16 weeks

of diet. (**E**) Total cholesterolemia of control and HFD mice at 16 weeks of diet. *P < 0.05, **P < 0.01, ***P < 0.001: control diet vs. HFD. Data are presented as means ± SEM.

2. Glucose homeostasis / Glucose regulation

Fasting glucose levels were assessed and exhibited a significant increase in HFD-fed mice compared to mice fed with the control diet (P < 0.001; **Figure 2A**). However, HbA1c levels were not significantly altered in mice fed with HFD compared to control diet-fed mice (**Figure 2B**). Plasma insulin level in HFD-fed mice was significantly increased compared to control mice (P < 0.001; **Figure 2C**) confirming impaired glucose tolerance and insulin resistance. We performed an oral glucose tolerance test (OGTT) after 16 weeks of diet on both groups. We observed that glucose tolerance was impaired in HFD-fed mice compared to control mice (**Figure 2D**) with the AUC of blood glucose concentration significantly higher in HFD-fed mice compared to control diet-fed mice (P < 0.01; **Figure 2E**).

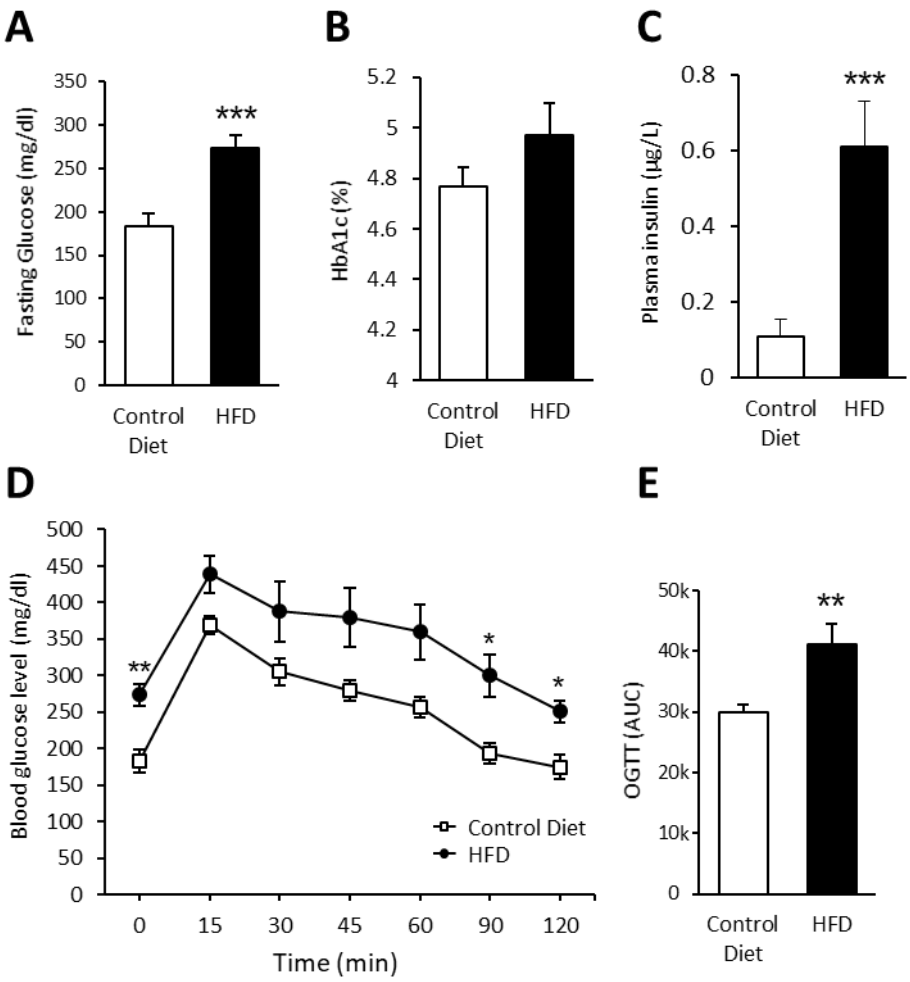

272 **Figure 2: HFD-induced impaired glucose tolerance. (A)** Fasting blood glucose of control diet-fed mice
273 and HFD-fed mice at 16 weeks of diet. **(B)** Percentage of glycated hemoglobin (HbA1c) of control diet-
274 fed mice and HFD-fed mice at 16 weeks of diet. **(C)** Plasma insulin of control diet-fed mice and HFD-
275 fed mice at 16 weeks of diet. **(D)** Oral glucose tolerance test (OGTT) curves performed at 16 weeks of
276 diet in control and HFD-fed mice. **(E)** Area under the curve (AUC) during OGTT for control diet-fed mice
277 and HFD-fed mice. *P < 0.05, **P < 0.01, ***P < 0.001: control diet vs. HFD. Data are presented as
278 means ± SEM (n=10/group).

279

280 *3. Nerve conduction studies*

281 At week 16, nerve conduction velocity (NCV) was measured in the sciatic and sural nerves of
282 each animal. HFD-fed mice did not show any significant change in motor (**Figure 3A**) or sensory
283 (**Figure 3B**) NCV compared to control mice.

284

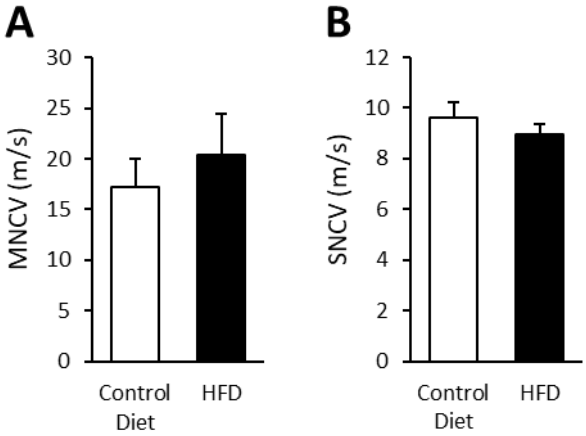

285

286 **Figure 3: Nerve conduction studies. (A)** Motor nerve conduction velocity (MNCV) performed at 16
287 weeks of diet in control and HFD-fed mice. **(B)** Sensory nerve conduction velocity (SNCV) performed at
288 16 weeks of diet in control and HFD-fed mice**.** Data are presented as means ± SEM (n=10/group).

289

290 *4. Thermal and mechanical pain sensitivity*

291 To evaluate peripheral neuropathy in mice we performed various behavioral sensory tests
292 every 4 weeks for 16 weeks of diet. HFD-fed mice exhibited an increase in paw withdrawal
293 threshold as early as 8 weeks (4 weeks HFD vs. 8 weeks HFD, P < 0.01, **Figure 4A**) and were
294 significantly different from their control diet-fed counterparts after 12 weeks of diet (12 weeks
295 control diet vs. 12 weeks HFD, P < 0.01, **Figure 4A**), indicating a decrease in mechanical
296 sensitivity. In parallel, we observed an increase in thermal sensitivity of HFD-fed mice
297 compared to control mice from week 8 (**Figure 4B**). The latency of hindpaw withdrawal in
298 response to noxious thermal stimulus was significantly decreased in HFD-fed mice compared
299 to control diet-fed mice at 12 and 16 weeks (P < 0.001). No significant change in haptic

300 mechanical sensitivity (**Figure 4C**) evaluated with the brush test or acute mechanical pain
301 sensitivity (**Figure 4D**) assessed by the pinprick test was noticed over 16 weeks between both
302 groups.

303

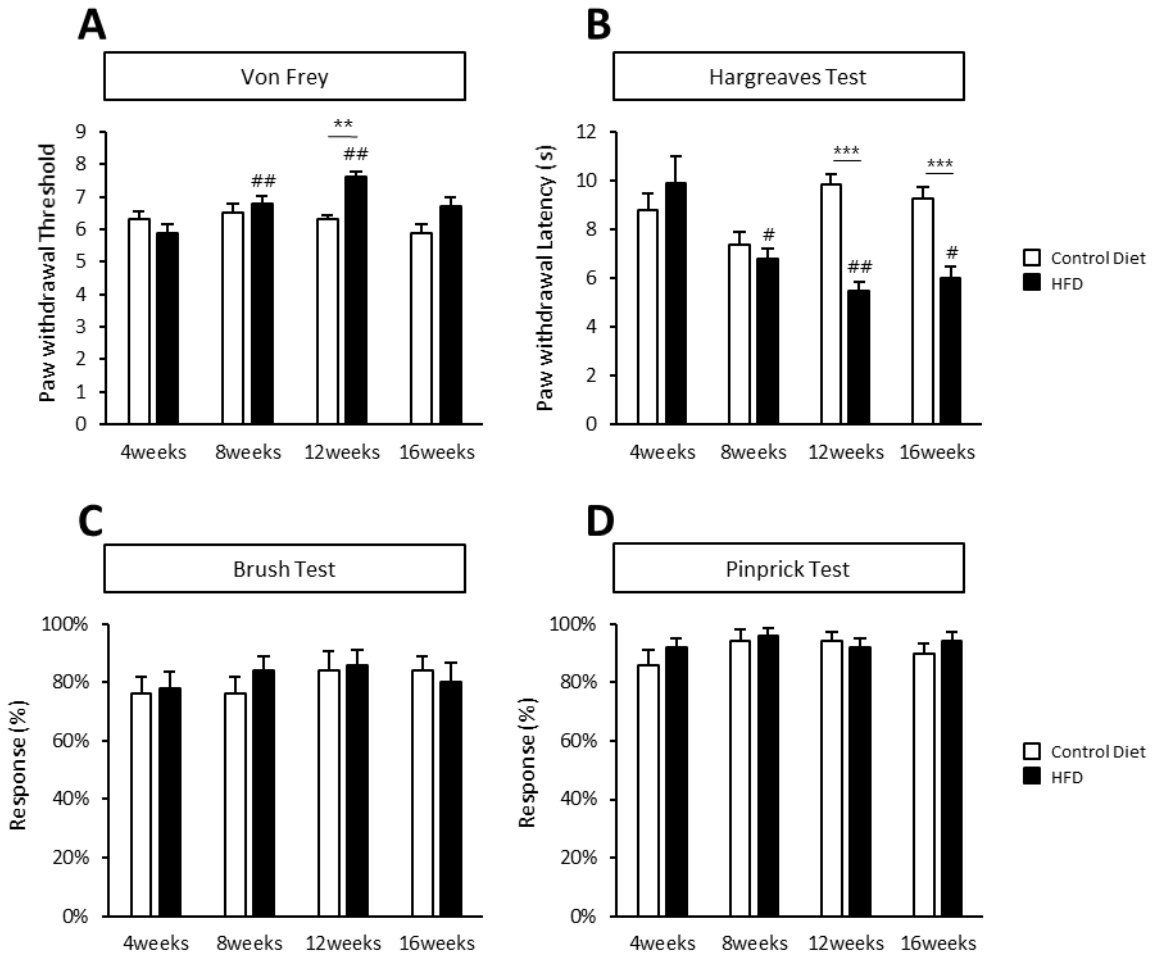

304

305 **Figure 4: Mechanical and thermal sensitivity changes induced by HFD. (A)** Quantification of static
306 mechanical sensitivity was assessed every 4 weeks in control and HFD-fed mice using von Frey
307 filaments. **(B)** Quantification of thermal sensitivity by Hargreaves test every 4 weeks in control and
308 HFD-fed mice. **(C)** Quantification of haptic mechanical sensitivity by brush test every 4 weeks in control
309 and HFD-fed mice. **(D)** Quantification of acute mechanical pain by pinprick test every 4 weeks in
310 control- and HFD-fed mice. $^{**}P < 0.01$, $^{***}P < 0.001$: control diet vs. HFD. #$P < 0.05$, ##$P < 0.01$: HFD
311 4weeks vs. HFD 8, 12 or 16 weeks. Data are presented as means ±SEM (n=10/group).

312

313 *5. Epidermal innervation and Nociceptive Schwann cells*

314 In order to fully characterized neuropathy in our model, we analyzed the intraepidermal nerve
315 fiber density (IENFD) in the glabrous skin of control and HFD-fed mice. Our results show a
316 significant reduction of foot skin innervation in HFD-fed compared with control mice after 16
317 weeks of diet ($P < 0.001$; **Figure 5A**, **5B**). Additionally, we investigated the integrity of

318 nociceptive Schwann cells that are present in the skin at the junction between the epidermis
319 and the dermis by using immunohistochemistry against the L1 Cell Adhesion Molecule
320 (L1CAM) that we found highly expressed in these cell types (**Supplementary Figure 1A, B**). To
321 validate the specificity of L1CAM expression in nociceptive Schwann cells, we first verified its
322 colocalization with Sox10 and S100β, two markers previously described to be expressed in
323 these cells (Hu et al., 2022; Ojeda-Alonso et al., 2023; Rinwa et al., 2021) (**Supplementary**
324 **Figure 1A**). To go even further, we confirmed the expression of L1CAM in Td-tomato positive
325 nSCs in PLP-CreER^{T2};Ai14 double transgenic mouse foot skin (**Supplementary Figure 1B**),
326 (Gomez-Sanchez et al., 2017; Leone et al., 2003). Altogether, these results indicate that L1CAM
327 is a reliable marker of nSCs.

328 Using L1CAM to identified nSCs, we observed that, both mean fluorescence intensity (**Figure**
329 **5C**,**D**) and mean number of L1CAM-positive cells and cellular extensions (**Figure 5C**,**E**) were
330 significantly decreased in HFD-fed mice compared with control mice ($P < 0.001$ and $P < 0.01$
331 respectively). Altogether, these results indicate a decrease in both sensory nerve endings and
332 nociceptive Schwann cells in the foot skin of HFD mice.

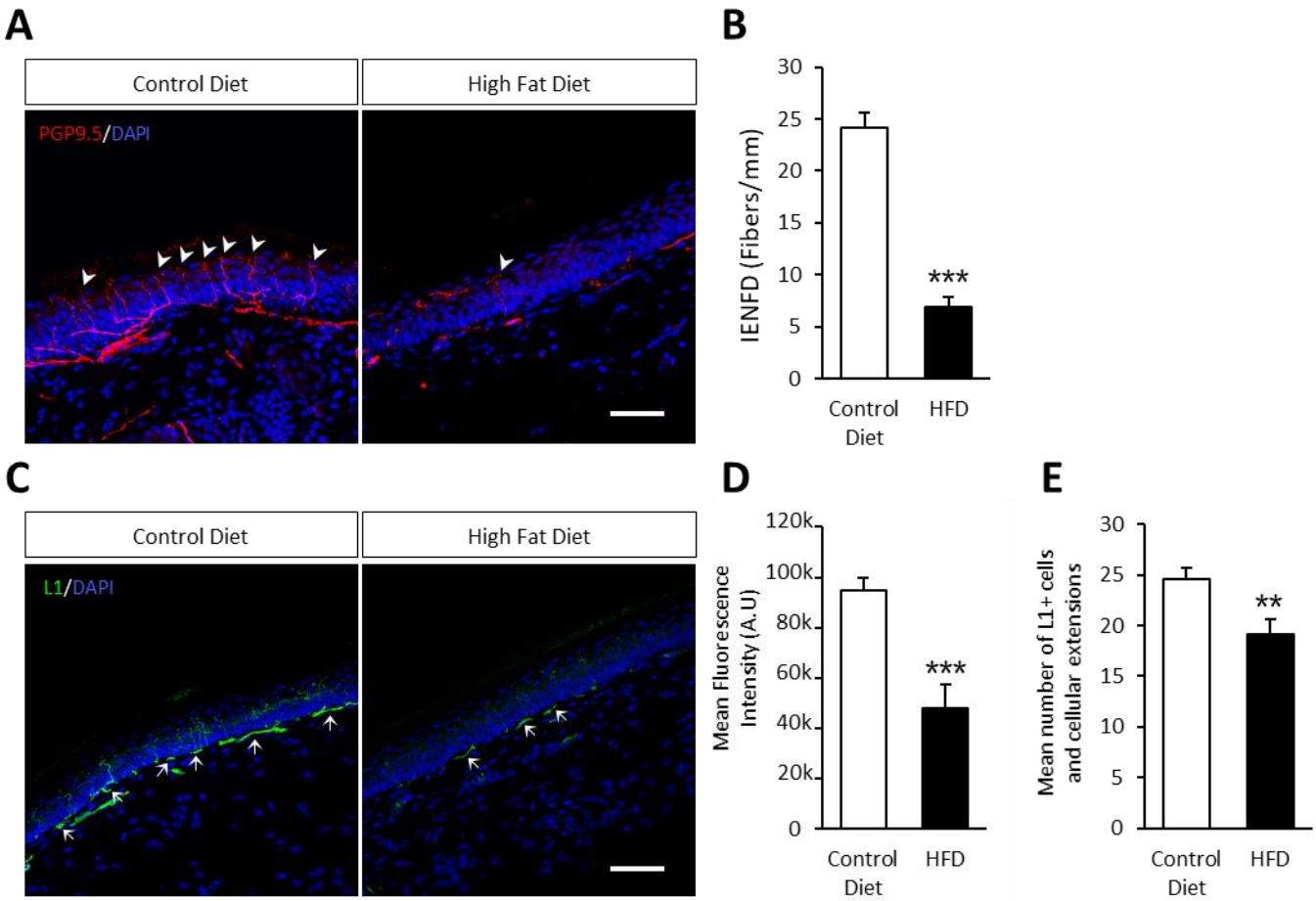

333

334 **Figure 5: HFD-induced small nerve fiber and nociceptive Schwann cells degeneration in the foot skin.**
335 **(A)** PGP9.5 immunofluorescence with DAPI staining in foot skin section of control (n=5) and HFD-fed
336 mice (n=5). **(B)** Quantitation of IENFD is presented as the number of fibers/mm of epidermis. **(C)** L1CAM
337 immunofluorescence with DAPI staining in foot skin section of control (n=5) and HFD-fed mice (n=5).

Arrowhead indicate nerve fibers in the epidermis of the foot skin. Arrows indicate nociceptive Schwann cells and their cellular extensions at the border of the epidermis and the dermis. **(D)** Mean fluorescence intensity quantification of L1CAM immunostaining at the localization of nociceptive Schwann cells (at the border of epidermis and dermis). **(E)** Quantification of L1CAM-positive cells and their cellular extensions presented in number/mm of epidermis. $^{**}P < 0.01$, $^{***}P < 0.001$: control diet vs. HFD. Data are presented as means ±SEM. Scale bar: 50 µm.

Discussion

In the present study, we used HFD (45% fat) fed mice during 16 weeks to generate a mouse model of peripheral neuropathy in prediabetic condition and compared dyslipidemia, glucose tolerance, and sensory deficits of the mice with the corresponding control diet (10% fat). We demonstrated that HFD-fed mice develop a prediabetic phenotype with increased weight gain, elevated leptinemia, hypercholesterolemia, impaired glucose tolerance, and elevated fasting blood glucose and insulin resistance compared with control mice. Our combined findings show that the HFD model recapitulate metabolic dysfunction observed in prediabetes. The analysis of IENFD of the foot skin revealed an important reduction of terminal fibers and nSCs in HFD-fed mice compared with mice fed with a control-diet. We also observed behavioral sensory deficits in HFD-fed mice, with the development of mechanical hyposensitivity and thermal hypersensitivity. Overall, our results indicate that HFD-fed mice exhibit peripheral neuropathy in prediabetic conditions.

The literature on HFD models is extensive and each diet seems to have its specificities, which leads to the development of different phenotypes in animals. Indeed, whether it is between high fat diets of 45 or 60% of fat or even on the composition of the diet between those using lard-based vs. plant-based or fish oil fats, the results obtained are not similar (For review see (Eid and Feldman, 2021)). Rodent studies using a 60% fat HFD are potentially not relevant as those using a 45% fat diet in term of human food consumption (Speakman, 2019). Therefore, the choice and a proper characterization of the diet is important to know where the model stands in terms of clinical significance. Mice fed on a high-fat diet progressively develop metabolic disorders, including weight gain, insulin resistance, dyslipidemia and impaired glucose tolerance. The HFD used in the present study recapitulates all of these deficits after 16 weeks of diet, with some discrepancies from the literature depending on the time spent on diet. Indeed, when mice are fed with HFD during 34 weeks they developed a more pronounced metabolic phenotype as demonstrated by increased plasma triglycerides (TG) and elevated glycated hemoglobin (Vincent et al., 2009; Xu et al., 2019) which we did not find in the present study. However, the lack of a difference in TG levels was also found in a similar study by Sajic and colleagues after the same time spent on HFD (16 weeks) (Sajic et al., 2021). For HbA1c levels, fasting blood glucose was only evaluated at the end of the experiments and, despite we demonstrated hyperglycemia in HFD-fed mice, we do not know since when chronic

377 hyperglycemia started. Importantly, glycation of hemoglobin starts 6 weeks following
378 persistent hyperglycemia on rats (Nagisa et al., 2003) and then last until the lifespan of the
379 red blood cell, which is about 3 months in human, 60 days in rats and 40 days in mice (Van
380 Putten, 1958). It is then possible that in our study the chronic hyperglycemia of HFD mice did
381 not last long enough to be able to have an impact on the level of glycated hemoglobin
382 evaluated at 16 weeks. Considering the other metabolic parameters we measured in our
383 study, we can assume that our HFD-fed mice were pre-diabetic.

384 To characterize the progression of peripheral neuropathy, we followed the guidelines of the
385 diabetic neuropathy study group of the European Association for the Study of Diabetes
386 (Neurodiab). Namely, we assessed three key features present in human pathology
387 (nocifensive behavior, nerve conduction velocity, and IENFD) considering that the presence of
388 alterations in two of these three assessments are necessary to establish neuropathy in rodents
389 (Biessels et al., 2014). In this study, we demonstrated that HFD-fed mice exhibited mechanical
390 hypoalgesia and thermal hyperalgesia coupled to a severe loss of intraepidermal nerve fibers
391 but no impairment of motor or sensory nerve conduction velocity. According to the criteria of
392 Neurodiab, we can assert that our HFD-fed mice develop peripheral neuropathy in a context
393 of prediabetes.

394 In order to identify possible damage to small sensory fibers, we performed a quantification of
395 intraepidermal nerve fibers density considered as the gold standard for the evaluation of small
396 fiber neuropathies (Yu, 2021). Damage to small sensory fibers is one of the earliest
397 manifestations of DPN that can be observed in prediabetic conditions (Sumner et al., 2003).
398 We found a drastic reduction of 70% of epidermal innervation in the hind paw of the HFD-fed
399 mice in comparison to control-fed mice. This reduction of nerve fibers density is in accordance
400 with the literature using an equivalent HFD (Coppey et al., 2011; Sajic et al., 2021; Vincent et
401 al., 2009). Studies have shown that small nerve fibers penetrating the epidermis are mostly
402 nociceptive (Lauria et al., 2022) and these fibers undergo degeneration and regeneration in
403 patients with impaired glucose tolerance and at the early stages of type 2 diabetes (Green et
404 al., 2010; Ziegler et al., 2014). Once neuropathy progresses, degenerated fibers do not
405 regenerate. However, not all authors agree that the severity of IENFD loss is correlated with
406 sensory deficits and disease severity (Arimura et al., 2013; Nolano et al., 2020; Shun et al.,
407 2004; Smith et al., 2001). Until recently, it was thought that because unmyelinated C-fibers
408 lack the protection and nutrient supply that myelinated Schwann cells provide to A-fibers,
409 these unmyelinated C-fibers were more likely to be affected at the early stages of diabetic
410 neuropathy. However, recently a specialized cutaneous type of Schwann cells, termed
411 nociceptive Schwann cells , in close relationship with nociceptive C-fibers in the dermis has
412 been discovered (Abdo et al., 2019). These cells contribute to terminal axon support and play
413 a critical role in skin mechanosensitivity and neuropathic pain (De Logu et al., 2017; Ojeda-
414 Alonso et al., 2023; Raut et al., 2024; Rinwa et al., 2021). Therefore, nociceptive endings in the
415 epidermis are not “free” but form a mesh-like organ with a mutual dependence between C-
416 fibers and the nSCs. The absence of nSCs induces a retraction of epidermal nerve fibers and

417 development of mechanical, cold, and heat hyperalgesia (Rinwa et al., 2021). In the present
418 study, we identified L1CAM as a reliable marker for nSCs, as an alternative to the conventional
419 S100β / Sox10 staining methods highlighted by (Hu et al., 2022; Ojeda-Alonso et al., 2023;
420 Rinwa et al., 2021). Interestingly, previous research used another cell adhesion molecule,
421 NCAM to identify terminal Schwann cells in the skin of diabetic patients (Reinisch et al., 2008).
422 As outlined by Hu et al., the precise localization of Schwann cells serves as a crucial criterion
423 in distinguishing nSCs (Hu et al., 2022). These distinctive cells are arranged within a 25 µm
424 depth in the subepidermal region, excluding glands and large fiber bundles. Based on these
425 criteria and the expression of L1CAM, we demonstrated a significant decrease in the number
426 of nSCs and their cellular extensions in HFD-fed mice compared to control mice. Interestingly,
427 a similar results was obtained in a mouse model of type 1 diabetes which develop mechanical
428 and thermal hyperalgesia (Hu et al., 2022).

429 Prediabetes represents the earliest stage of glucose dysregulation and hyperglycemia a
430 primary factor that can induces apoptosis in Schwann cells (Liu et al., 2020). High glucose levels
431 found in diabetic patients can lead to oxidative stress, inflammatory reactions, endoplasmic
432 reticulum stress, autophagy, nitrification, and disruption of various signaling pathways such
433 as PI3K/AKT, ERK, PERK/Nrf2, and Wnt/β-catenin, all of which are involved in Schwann cells
434 apoptosis and the pathogenesis of DPN (Li et al., 2017; Liu et al., 2020; Wu et al., 2023; Zhang
435 et al., 2021). Inhibiting apoptosis of Schwann cells under high-glucose conditions is considered
436 a promising approach to treat DPN (Wang et al., 2023). While glycemic control has little impact
437 of the development and progression of neuropathy in type 2 diabetic patients (Callaghan et
438 al., 2012b), it is important to recognize that DPN is influenced by various metabolic
439 parameters. In addition to elevated glucose levels, dyslipidemia is another factor commonly
440 observed in diabetic patients and despite its prevalence, the impact of dyslipidemia on
441 Schwann cells integrity has received relatively little attention into the literature (Jende et al.,
442 2019; Rumora et al., 2022; Stino et al., 2020). Overall, the above-mentioned literature focused
443 on Schwann cells in general, without any particular attention to the subpopulation of
444 nociceptive Schwann cells despite its major role in skin mechanosensitivity and neuropathic
445 pain. Therefore, the elucidation of mechanisms implicated in the alteration of nSCs in the skin
446 is crucial for understanding and developing potential treatments for DPN.

447

448 **Conclusion**

449 In this study, we used HFD to induce a mouse model of peripheral neuropathy in prediabetic
450 condition. We observed key metabolic dysfunctions associated with prediabetes, including
451 increased weight gain, hypercholesterolemia, and impaired glucose tolerance. Behavioral
452 analysis uncovered early-onset of peripheral neuropathy with mechanical hypoalgesia and
453 thermal hyperalgesia. We also identified L1CAM as a new marker of nociceptive Schwann cells
454 previously characterized by the expression of S100β and Sox10. Interestingly, we observed a
455 significant decrease in number of nociceptive Schwann cells and their extensions in the foot

skin of neuropathic mice, highlighting the vulnerability of these cells in prediabetic conditions. Overall, this research enhances our understanding of the early events in peripheral neuropathy during prediabetic states, paving the way for future investigations into the molecular mechanisms underlying nociceptive Schwann cells alterations and potential strategies to thwart this complication of diabetes.

466 **Bibliography**

467 Abdo, H., Calvo-Enrique, L., Lopez, J.M., Song, J., Zhang, M.-D., Usoskin, D., El Manira, A., Adameyko,
468 I., Hjerling-Leffler, J., Ernfors, P., 2019. Specialized cutaneous Schwann cells initiate pain
469 sensation. Science 365, 695–699. https://doi.org/10.1126/science.aax6452
470 Arimura, A., Deguchi, T., Sugimoto, K., Uto, T., Nakamura, T., Arimura, Y., Arimura, K., Yagihashi, S.,
471 Nishio, Y., Takashima, H., 2013. Intraepidermal nerve fiber density and nerve conduction
472 study parameters correlate with clinical staging of diabetic polyneuropathy. Diabetes Res.
473 Clin. Pract. 99, 24–29. https://doi.org/10.1016/j.diabres.2012.09.026
474 Biessels, G.J., Bril, V., Calcutt, N.A., Cameron, N.E., Cotter, M.A., Dobrowsky, R., Feldman, E.L.,
475 Fernyhough, P., Jakobsen, J., Malik, R.A., Mizisin, A.P., Oates, P.J., Obrosova, I.G., Pop-Busui,
476 R., Russell, J.W., Sima, A.A., Stevens, M.J., Schmidt, R.E., Tesfaye, S., Veves, A., Vinik, A.I.,
477 Wright, D.E., Yagihashi, S., Yorek, M.A., Ziegler, D., Zochodne, D.W., 2014. Phenotyping
478 animal models of diabetic neuropathy: a consensus statement of the diabetic neuropathy
479 study group of the EASD (Neurodiab). J. Peripher. Nerv. Syst. JPNS 19, 77–87.
480 https://doi.org/10.1111/jns5.12072
481 Bonin, R.P., Bories, C., De Koninck, Y., 2014. A simplified up-down method (SUDO) for measuring
482 mechanical nociception in rodents using von Frey filaments. Mol. Pain 10, 26.
483 https://doi.org/10.1186/1744-8069-10-26
484 Bourane, S., Grossmann, K.S., Britz, O., Dalet, A., Del Barrio, M.G., Stam, F.J., Garcia-Campmany, L.,
485 Koch, S., Goulding, M., 2015. Identification of a spinal circuit for light touch and fine motor
486 control. Cell 160, 503–515. https://doi.org/10.1016/j.cell.2015.01.011
487 Callaghan, B.C., Cheng, H.T., Stables, C.L., Smith, A.L., Feldman, E.L., 2012a. Diabetic neuropathy:
488 clinical manifestations and current treatments. Lancet Neurol. 11, 521–534.
489 https://doi.org/10.1016/S1474-4422(12)70065-0
490 Callaghan, B.C., Little, A.A., Feldman, E.L., Hughes, R.A.C., 2012b. Enhanced glucose control for
491 preventing and treating diabetic neuropathy. Cochrane Database Syst. Rev. 6, CD007543.
492 https://doi.org/10.1002/14651858.CD007543.pub2
493 Coppey, L., Davidson, E., Lu, B., Gerard, C., Yorek, M., 2011. Vasopeptidase inhibitor ilepatril
494 (AVE7688) prevents obesity- and diabetes-induced neuropathy in C57Bl/6J mice.
495 Neuropharmacology 60, 259–266. https://doi.org/10.1016/j.neuropharm.2010.09.008
496 De Logu, F., Nassini, R., Materazzi, S., Carvalho Gonçalves, M., Nosi, D., Rossi Degl'Innocenti, D.,
497 Marone, I.M., Ferreira, J., Li Puma, S., Benemei, S., Trevisan, G., Souza Monteiro de Araújo,
498 D., Patacchini, R., Bunnett, N.W., Geppetti, P., 2017. Schwann cell TRPA1 mediates
499 neuroinflammation that sustains macrophage-dependent neuropathic pain in mice. Nat.
500 Commun. 8, 1887. https://doi.org/10.1038/s41467-017-01739-2
501 Deuis, J.R., Vetter, I., 2016. The thermal probe test: A novel behavioral assay to quantify thermal paw
502 withdrawal thresholds in mice. Temp. Multidiscip. Biomed. J. 3, 199–207.
503 https://doi.org/10.1080/23328940.2016.1157668
504 Doerflinger, N.H., Macklin, W.B., Popko, B., 2003. Inducible site-specific recombination in myelinating
505 cells. genesis 35, 63–72. https://doi.org/10.1002/gene.10154
506 Eid, S.A., Feldman, E.L., 2021. Advances in diet-induced rodent models of metabolically acquired
507 peripheral neuropathy. Dis. Model. Mech. 14, dmm049337.
508 https://doi.org/10.1242/dmm.049337
509 Feldman, E.L., Nave, K.-A., Jensen, T.S., Bennett, D.L.H., 2017. New Horizons in Diabetic Neuropathy:
510 Mechanisms, Bioenergetics, and Pain. Neuron 93, 1296–1313.
511 https://doi.org/10.1016/j.neuron.2017.02.005
512 Gomez-Sanchez, J.A., Pilch, K.S., van der Lans, M., Fazal, S.V., Benito, C., Wagstaff, L.J., Mirsky, R.,
513 Jessen, K.R., 2017. After Nerve Injury, Lineage Tracing Shows That Myelin and Remak
514 Schwann Cells Elongate Extensively and Branch to Form Repair Schwann Cells, Which Shorten
515 Radically on Remyelination. J. Neurosci. Off. J. Soc. Neurosci. 37, 9086–9099.
516 https://doi.org/10.1523/JNEUROSCI.1453-17.2017

517 Green, A.Q., Krishnan, S., Finucane, F.M., Rayman, G., 2010. Altered C-fiber function as an indicator
518 of early peripheral neuropathy in individuals with impaired glucose tolerance. Diabetes Care
519 33, 174–176. https://doi.org/10.2337/dc09-0101
520 Grove, M., Kim, H., Santerre, M., Krupka, A.J., Han, S.B., Zhai, J., Cho, J.Y., Park, R., Harris, M., Kim, S.,
521 Sawaya, B.E., Kang, S.H., Barbe, M.F., Cho, S.-H., Lemay, M.A., Son, Y.-J., 2017. YAP/TAZ
522 initiate and maintain Schwann cell myelination. eLife 6, e20982.
523 https://doi.org/10.7554/eLife.20982
524 Hargreaves, K., Dubner, R., Brown, F., Flores, C., Joris, J., 1988. A new and sensitive method for
525 measuring thermal nociception in cutaneous hyperalgesia. Pain 32, 77–88.
526 https://doi.org/10.1016/0304-3959(88)90026-7
527 Hu, X., Agarwal, N., Zhang, M.-D., Ernfors, P., Kuner, R., Nyengaard, J.R., Karlsson, P., 2022.
528 Identification and quantification of nociceptive Schwann cells in mice with and without
529 Streptozotocin-induced diabetes. J. Chem. Neuroanat. 123, 102118.
530 https://doi.org/10.1016/j.jchemneu.2022.102118
531 Jende, J.M.E., Groener, J.B., Rother, C., Kender, Z., Hahn, A., Hilgenfeld, T., Juerchott, A., Preisner, F.,
532 Heiland, S., Kopf, S., Pham, M., Nawroth, P., Bendszus, M., Kurz, F.T., 2019. Association of
533 Serum Cholesterol Levels With Peripheral Nerve Damage in Patients With Type 2 Diabetes.
534 JAMA Netw. Open 2, e194798. https://doi.org/10.1001/jamanetworkopen.2019.4798
535 Lauria, G., Faber, C.G., Cornblath, D.R., 2022. Skin biopsy and small fibre neuropathies: facts and
536 thoughts 30 years later. J. Neurol. Neurosurg. Psychiatry jnnp-2021-327742.
537 https://doi.org/10.1136/jnnp-2021-327742
538 Leone, D.P., Genoud, S., Atanasoski, S., Grausenburger, R., Berger, P., Metzger, D., Macklin, W.B.,
539 Chambon, P., Suter, U., 2003. Tamoxifen-inducible glia-specific Cre mice for somatic
540 mutagenesis in oligodendrocytes and Schwann cells. Mol. Cell. Neurosci. 22, 430–440.
541 https://doi.org/10.1016/s1044-7431(03)00029-0
542 Li, R., Wu, Y., Zou, S., Wang, X., Li, Y., Xu, K., Gong, F., Liu, Y., Wang, J., Liao, Y., Li, X., Xiao, J., 2017.
543 NGF Attenuates High Glucose-Induced ER Stress, Preventing Schwann Cell Apoptosis by
544 Activating the PI3K/Akt/GSK3β and ERK1/2 Pathways. Neurochem. Res. 42, 3005–3018.
545 https://doi.org/10.1007/s11064-017-2333-6
546 Liu, Y.-P., Shao, S.-J., Guo, H.-D., 2020. Schwann cells apoptosis is induced by high glucose in diabetic
547 peripheral neuropathy. Life Sci. 248, 117459. https://doi.org/10.1016/j.lfs.2020.117459
548 Malik, R.A., Tesfaye, S., Newrick, P.G., Walker, D., Rajbhandari, S.M., Siddique, I., Sharma, A.K.,
549 Boulton, A.J.M., King, R.H.M., Thomas, P.K., Ward, J.D., 2005. Sural nerve pathology in
550 diabetic patients with minimal but progressive neuropathy. Diabetologia 48, 578–585.
551 https://doi.org/10.1007/s00125-004-1663-5
552 Margolis, D.J., Malay, D.S., Hoffstad, O.J., Leonard, C.E., MaCurdy, T., de Nava, K.L., Tan, Y., Molina,
553 T., Siegel, K.L., 2011. Incidence of diabetic foot ulcer and lower extremity amputation among
554 Medicare beneficiaries, 2006 to 2008: Data Points #2, in: Data Points Publication Series.
555 Agency for Healthcare Research and Quality (US), Rockville (MD).
556 Nagisa, Y., Kato, K., Watanabe, K., Murakoshi, H., Odaka, H., Yoshikawa, K., Sugiyama, Y., 2003.
557 Changes in glycated haemoglobin levels in diabetic rats measured with an automatic affinity
558 HPLC. Clin. Exp. Pharmacol. Physiol. 30, 752–758. https://doi.org/10.1046/j.1440-
559 1681.2003.03902.x
560 Nolano, M., Tozza, S., Caporaso, G., Provitera, V., 2020. Contribution of Skin Biopsy in Peripheral
561 Neuropathies. Brain Sci. 10, 989. https://doi.org/10.3390/brainsci10120989
562 Obrosova, I.G., Li, F., Abatan, O.I., Forsell, M.A., Komjáti, K., Pacher, P., Szabó, C., Stevens, M.J., 2004.
563 Role of poly(ADP-ribose) polymerase activation in diabetic neuropathy. Diabetes 53, 711–
564 720. https://doi.org/10.2337/diabetes.53.3.711
565 Oh, S.S., Hayes, J.M., Sims-Robinson, C., Sullivan, K.A., Feldman, E.L., 2010. The effects of anesthesia
566 on measures of nerve conduction velocity in male C57Bl6/J mice. Neurosci. Lett. 483, 127–
567 131. https://doi.org/10.1016/j.neulet.2010.07.076

568 Ojeda-Alonso, J., Calvo-Enrique, L., Paricio-Montesinos, R., Kumar, R., Zhang, M.-D., Poulet, J.F.A.,
569 Ernfors, P., Lewin, G.R., 2023. Sensory Schwann cells set perceptual thresholds for touch and
570 selectively regulate mechanical nociception. https://doi.org/10.1101/2022.02.04.477749
571 Raut, N.G.R., Maile, L.A., Oswalt, L.M., Mitxelena, I., Adlakha, A., Sprague, K.L., Rupert, A.R., Bokros,
572 L., Hofmann, M.C., Patritti-Cram, J., Rizvi, T.A., Queme, L.F., Choi, K., Ratner, N., Jankowski,
573 M.P., 2024. Schwann cells modulate nociception in neurofibromatosis 1. JCI Insight 9.
574 https://doi.org/10.1172/jci.insight.171275
575 Reinisch, C.M., Traxler, H., Piringer, S., Tangl, S., Nader, A., Tschachler, E., 2008. Rarefaction of the
576 Peripheral Nerve Network in Diabetic Patients Is Associated With a Pronounced Reduction of
577 Terminal Schwann Cells. Diabetes Care 31, 1219–1221. https://doi.org/10.2337/dc07-1832
578 Rinwa, P., Calvo-Enrique, L., Zhang, M.-D., Nyengaard, J.R., Karlsson, P., Ernfors, P., 2021. Demise of
579 nociceptive Schwann cells causes nerve retraction and pain hyperalgesia. Pain 162, 1816–
580 1827. https://doi.org/10.1097/j.pain.0000000000002169
581 Rumora, A.E., Kim, B., Feldman, E.L., 2022. A Role for Fatty Acids in Peripheral Neuropathy Associated
582 with Type 2 Diabetes and Prediabetes. Antioxid. Redox Signal. 37, 560–577.
583 https://doi.org/10.1089/ars.2021.0155
584 Sajic, M., Rumora, A.E., Kanhai, A.A., Dentoni, G., Varatharajah, S., Casey, C., Brown, R.D.R., Peters, F.,
585 Hinder, L.M., Savelieff, M.G., Feldman, E.L., Smith, K.J., 2021. High Dietary Fat Consumption
586 Impairs Axonal Mitochondrial Function In Vivo. J. Neurosci. 41, 4321–4334.
587 https://doi.org/10.1523/JNEUROSCI.1852-20.2021
588 Schulz, A., Walther, C., Morrison, H., Bauer, R., 2014. In vivo electrophysiological measurements on
589 mouse sciatic nerves. J. Vis. Exp. JoVE 51181. https://doi.org/10.3791/51181
590 Shun, C.-T., Chang, Y.-C., Wu, H.-P., Hsieh, S.-C., Lin, W.-M., Lin, Y.-H., Tai, T.-Y., Hsieh, S.-T., 2004.
591 Skin denervation in type 2 diabetes: correlations with diabetic duration and functional
592 impairments. Brain J. Neurol. 127, 1593–1605. https://doi.org/10.1093/brain/awh180
593 Smith, A.G., Ramachandran, P., Tripp, S., Singleton, J.R., 2001. Epidermal nerve innervation in
594 impaired glucose tolerance and diabetes-associated neuropathy. Neurology 57, 1701–1704.
595 https://doi.org/10.1212/wnl.57.9.1701
596 Speakman, J.R., 2019. Use of high-fat diets to study rodent obesity as a model of human obesity. Int.
597 J. Obes. 2005 43, 1491–1492. https://doi.org/10.1038/s41366-019-0363-7
598 Stino, A.M., Rumora, A.E., Kim, B., Feldman, E.L., 2020. Evolving concepts on the role of dyslipidemia,
599 bioenergetics, and inflammation in the pathogenesis and treatment of diabetic peripheral
600 neuropathy. J. Peripher. Nerv. Syst. JPNS 25, 76–84. https://doi.org/10.1111/jns.12387
601 Sumner, C.J., Sheth, S., Griffin, J.W., Cornblath, D.R., Polydefkis, M., 2003. The spectrum of
602 neuropathy in diabetes and impaired glucose tolerance. Neurology 60, 108–111.
603 https://doi.org/10.1212/wnl.60.1.108
604 Themistocleous, A.C., Ramirez, J.D., Shillo, P.R., Lees, J.G., Selvarajah, D., Orengo, C., Tesfaye, S., Rice,
605 A.S.C., Bennett, D.L.H., 2016. The Pain in Neuropathy Study (PiNS): a cross-sectional
606 observational study determining the somatosensory phenotype of painful and painless
607 diabetic neuropathy. Pain 157, 1132–1145.
608 https://doi.org/10.1097/j.pain.0000000000000491
609 Van Putten, L.M., 1958. The life span of red cells in the rat and the mouse as determined by labeling
610 with DFP32 in vivo. Blood 13, 789–794.
611 Vincent, A.M., Hayes, J.M., McLean, L.L., Vivekanandan-Giri, A., Pennathur, S., Feldman, E.L., 2009.
612 Dyslipidemia-induced neuropathy in mice: the role of oxLDL/LOX-1. Diabetes 58, 2376–2385.
613 https://doi.org/10.2337/db09-0047
614 Wang, X., Xu, G., Liu, H., Chen, Z., Huang, S., Yuan, J., Xie, C., Du, L., 2023. Inhibiting apoptosis of
615 Schwann cell under the high-glucose condition: A promising approach to treat diabetic
616 peripheral neuropathy using Chinese herbal medicine. Biomed. Pharmacother. 157, 114059.
617 https://doi.org/10.1016/j.biopha.2022.114059

618 Wu, K., Deng, F., Mao, X., Zhou, D., Shen, W., 2023. Ferroptosis involves in Schwann cell death in
619 diabetic peripheral neuropathy. Open Med. 18, 20230809. https://doi.org/10.1515/med-
620 2023-0809
621 Xu, L., Lin, X., Guan, M., Zeng, Y., Liu, Y., 2019. Verapamil Attenuated Prediabetic Neuropathy in High-
622 Fat Diet-Fed Mice through Inhibiting TXNIP-Mediated Apoptosis and Inflammation. Oxid.
623 Med. Cell. Longev. 2019, 1896041. https://doi.org/10.1155/2019/1896041
624 Yeomans, D.C., Proudfit, H.K., 1996. Nociceptive responses to high and low rates of noxious
625 cutaneous heating are mediated by different nociceptors in the rat: electrophysiological
626 evidence. Pain 68, 141–150. https://doi.org/10.1016/S0304-3959(96)03177-6
627 Yu, Y., 2021. Gold Standard for Diagnosis of DPN. Front. Endocrinol. 12, 719356.
628 https://doi.org/10.3389/fendo.2021.719356
629 Zhang, X., Zhao, S., Yuan, Q., Zhu, L., Li, F., Wang, H., Kong, D., Hao, J., 2021. TXNIP, a novel key factor
630 to cause Schwann cell dysfunction in diabetic peripheral neuropathy, under the regulation of
631 PI3K/Akt pathway inhibition-induced DNMT1 and DNMT3a overexpression. Cell Death Dis.
632 12, 1–13. https://doi.org/10.1038/s41419-021-03930-2
633 Ziegler, D., Papanas, N., Zhivov, A., Allgeier, S., Winter, K., Ziegler, I., Brüggemann, J., Strom, A.,
634 Peschel, S., Köhler, B., Stachs, O., Guthoff, R.F., Roden, M., German Diabetes Study (GDS)
635 Group, 2014. Early detection of nerve fiber loss by corneal confocal microscopy and skin
636 biopsy in recently diagnosed type 2 diabetes. Diabetes 63, 2454–2463.
637 https://doi.org/10.2337/db13-1819
638

639

640

641 **Figure Legends**

642

643 **Figure 1: Study design and HFD-induced dyslipidemia.** (**A**) Study Design used to assess the
644 effect of a HFD (45% kcal %fat) vs. a control diet (10% kcal %fat) in two groups of mice
645 (n=10/group). (**B**) Body weight of control diet-fed mice and HFD-fed mice during the 16 weeks
646 of diet. (**C**) Leptinemia of control and HFD mice at 16 weeks of diet. (**D**) Plasma levels
647 triglycerides of control and HFD mice at 16 weeks of diet. (**E**) Total cholesterolemia of control
648 and HFD mice at 16 weeks of diet. *P < 0.05, **P < 0.01, ***P < 0.001: control diet vs. HFD.
649 Data are presented as means ± SEM.

650

651 **Figure 2: HFD-induced impaired glucose tolerance. (A)** Fasting blood glucose of control diet-
652 fed mice and HFD-fed mice at 16 weeks of diet. **(B)** Percentage of glycated hemoglobin
653 (HbA1c) of control diet-fed mice and HFD-fed mice at 16 weeks of diet. **(C)** Plasma insulin of
654 control diet-fed mice and HFD-fed mice at 16 weeks of diet. **(D)** Oral glucose tolerance test
655 (OGTT) curves performed at 16 weeks of diet in control and HFD-fed mice. **(E)** Area under the
656 curve (AUC) during OGTT for control diet-fed mice and HFD-fed mice. *P < 0.05, **P < 0.01,
657 ***P < 0.001: control diet vs. HFD. Data are presented as means ± SEM (n=10/group).

658

659 **Figure 3: Nerve conduction studies. (A)** Motor nerve conduction velocity (MNCV) performed
660 at 16 weeks of diet in control and HFD-fed mice. **(B)** Sensory nerve conduction velocity (SNCV)
661 performed at 16 weeks of diet in control and HFD-fed mice**.** Data are presented as means ±
662 SEM (n=10/group).

663

664 **Figure 4: Mechanical and thermal sensitivity changes induced by HFD. (A)** Quantification of
665 static mechanical sensitivity was assessed every 4 weeks in control and HFD-fed mice using
666 von Frey filaments. **(B)** Quantification of thermal sensitivity by Hargreaves test every 4 weeks
667 in control and HFD-fed mice. **(C)** Quantification of haptic mechanical sensitivity by brush test
668 every 4 weeks in control and HFD-fed mice. **(D)** Quantification of acute mechanical pain by
669 pinprick test every 4 weeks in control- and HFD-fed mice. **P < 0.01, ***P < 0.001: control
670 diet vs. HFD. #P < 0.05, ##P < 0.01: HFD 4weeks vs. HFD 8, 12 or 16 weeks. Data are presented
671 as means ±SEM (n=10/group).

672

673 **Figure 5: HFD-induced small nerve fiber and nociceptive Schwann cells degeneration in the**
674 **foot skin. (A)** PGP9.5 immunofluorescence with DAPI staining in foot skin section of control
675 (n=5) and HFD-fed mice (n=5). **(B)** Quantitation of IENFD is presented as the number of
676 fibers/mm of epidermis. **(C)** L1CAM immunofluorescence with DAPI staining in foot skin

677 section of control (n=5) and HFD-fed mice (n=5). Arrowhead indicate nerve fibers in the
678 epidermis of the foot skin. Arrows indicate nociceptive Schwann cells and their cellular
679 extensions at the border of the epidermis and the dermis. **(D)** Mean fluorescence intensity
680 quantification of L1CAM immunostaining at the localization of nociceptive Schwann cells (at
681 the border of epidermis and dermis). **(E)** Quantification of L1CAM-positive cells and their
682 cellular extensions presented in number/mm of epidermis. $^{**}P < 0.01$, $^{***}P < 0.001$: control
683 diet vs. HFD. Data are presented as means ±SEM. Scale bar: 50 µm.

684

685 **Supplementary Figure 1: Colocalization of classical nociceptive Schwann cell markers with**
686 **L1CAM. (A)** L1CAM immunofluorescence colocalized with Sox10 and S100β classical markers
687 of nociceptive Schwann cells in the foot skin. **(B)** L1CAM immunofluorescence colocalized with
688 Td-tomato expressing nociceptive Schwann cells in a tamoxifen-induced PLP-*Cre*ER^{T2};
689 R26TdTomato double transgenic mouse. White arrows head indicate nociceptive Schwann
690 cells and their cellular extensions at the border of the epidermis and dermis. Scale bar: 50 µm.

691

692